Macromolecules

Article

pubs.acs.org/Macromolecules

Nitroxide-Mediated Polymerization of Styrenic Triarylamines and Chain-End Functionalization with a Ruthenium Complex: Toward Tailored Photoredox-Active Architectures

Robert Schroot, Christian Friebe, Esra Altuntas, Sarah Crotty, Michael Jäger,* and Ulrich S. Schubert*

Laboratory of Organic and Macromolecular Chemistry (IOMC), Friedrich-Schiller-University Jena, Humboldtstr. 10, 07743 Jena, Germany, and Jena Center for Soft Matter (JCSM), Philosophenweg 7 07743, Jena, Germany

Supporting Information

ABSTRACT: The preparation of redox-active polymers and the chain-end functionalization with one ruthenium complex was investigated in detail. A series of substituted monomers, i.e., styrenic triarylamines bearing methyl, fluoro, or methoxy substituents, were prepared by a one-pot Hartwig–Buchwald coupling. The nitroxide-mediated polymerization (NMP) was studied by variation of the functional initiators, the monomer-to-initiator ratios, and the solvent. The kinetic analysis of the prototypical methyl-substituted triarylamine shows the controlled polymerization up to 75% conversion, but a considerable decrease of the polymerization rate was observed during the course of the reaction. Both chain-end functionalities of the purified oligomers were subsequently utilized, i.e., the nitroxide to serve as a macroinitiator for an additional NMP step and the chloromethyl group to introduce one ruthenium complex at the chain terminus. The products were analyzed in detail by size-exclusion chromatography, NMR spectroscopy, and mass spectrometry. The optical and electrochemical properties of the prepared poly(triarylamine)s show the application potential as charge transport materials in conjunction with the photoactive ruthenium complex.

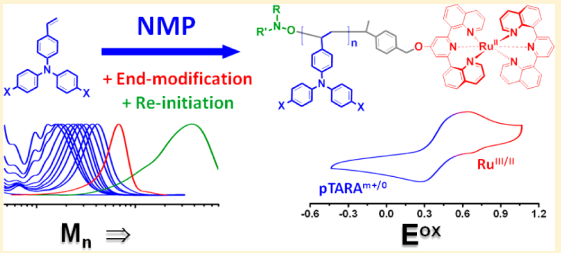

INTRODUCTION

The development of materials that harness light energy to generate a redox-chemical potential is the key to a modern sustainable energy supply. In general, the working principle involves the absorption of light to create an excited state (exciton), followed by charge separation, and ultimately the accumulation of redox equivalents. However, the efficient conversion of the transient excitation energy requires a well-tuned interplay of the elementary steps to compete with any unproductive back-reactions. In this regard, modern controlled radical polymerization techniques provide powerful methodologies to design and prepare such photo- and redox-active materials,[1−3] as shown by the rapid progress of organic photovoltaics[4−7] or (hybrid) storage systems.[8,9] In particular, the possibility to connect multiple (active) units provides the basis to mimic charge transport and accumulation processes also on a molecular level. In this regard, many (small) organic molecules can serve as redox-active components in electron-transfer reactions.[10] Noteworthy, the resulting transfer steps can be very efficient if such units are held close to each other, e.g., by the backbone to restrict the conformational freedom. For example, *para*-substituted styrenic triarylamines are attractive monomer candidates for electron-donor polymers due to their inherent good conducting properties[11−13] and redox stability[14] as well as the possibility to tune the redox potentials on a molecular level by peripheral substituents. [In this article, the term "polymer" is used consistently for clarity, although the term "oligomer" may be occasionally more appropriate.] In addition, the desired monomers can be readily polymerized in a controlled fashion by reversible addition–fragmentation chain-transfer (RAFT) polymerization[13,15,16] or nitroxide-mediated polymerization (NMP).[11,12,17] The latter technique offers the advantage to directly access telechelic polymers[18] by means of unimolecular radical initiators, but it generally requires higher reaction temperatures and the use of particularly reactive nitroxides,[3] e.g., 2,2,5-trimethyl-4-phenyl-3-azahexane-3-nitroxide (TIPNO) and *N*-(2-methylpropyl)-*N*-(1-diethylphosphono-2,2-dimethylpropyl)-*N*-oxyl (SG1). If the complementary initiator fragment contains a functional group, its modification enables the defined introduction of functional components at the chain terminus. A few NMP initiators are commercially available to fulfill this task, e.g., SG1 equipped with methacrylic acid (MAA), which can be modified prior to polymerization,[19] or TIPNO attached to chloromethylstyrene (CMSt), which is readily exploited by nucleophilic substitution.

In this contribution, the assembly of a redoxactive polymer and the subsequent attachment of a terminal photoactive unit (dye) are presented (Scheme 1). Within this architecture the dye carries out the charge separation and the injection into the adjacent redoxactive chain. Ruthenium polypyridyl-type complexes are attractive photoactive units due to their favorable combination of absorption of visible light, formation of long-

Received: December 25, 2012
Revised: January 31, 2013

Scheme 1. General Assembly Strategy of the Telechelic Redox-Active Macromolecules via Polymerization, Chain Extension, and End-Group Modification with a Photoredox-Active Dye

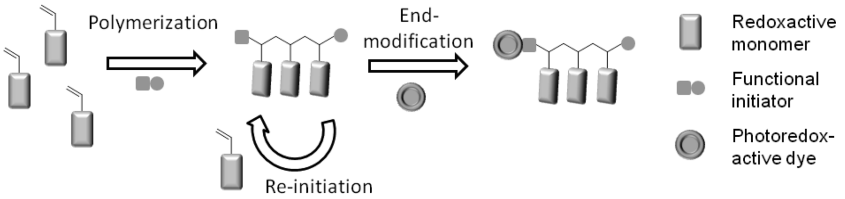

lived excited states, suitable redox potentials, chemical stability in the different oxidation states, and facile functionalization via the ligand scaffold.[20,21] In addition to the extensive fundamental studies of electron-transfer processes in molecular assemblies,[10,22,23] there is a continuing interest to utilize this class of compounds in macromolecules with light-harvesting and redox-active units.[24] An instructive review by Meyer et al. describes the development of ruthenium-based polymeric architectures, including their in-depth photophysical analysis and molecular modeling.[25] Noteworthy, an efficient charge separation is achieved by placing the redox-active units in close proximity. However, the quest of subsequent efficient vectorial charge transfer and accumulation of the redox equivalents is challenging due to trapping and recombination of charges within the statistical copolymer architecture. The placement of the photoredox-active unit in between a donor chain and an acceptor chain would, in principle, allow for unidirectional migration of the separated charges. The success of this design relies on the precise chain-end modification of the redox-active polymers. Hence, the design and synthetic approach of the target architecture are based on the following criteria: (1) Triarylamines-containing monomers are selected to ensure quantitative functionalization in the latter polymer, while the attached vinyl group ensures minimal spatial separation of the redox-active polymer with maximal through-space interaction.[26,27] (2) A novel $Ru^{II}(dqp)_2$-based (dqp is 2,6-di(quinolin-8-yl)pyridine) complex serves as the photoactive unit, which typically displays excited-state lifetimes in the microsecond time scale at room temperature.[28−30] (3) The nitroxide-mediated polymerization using functional initiators allows the direct preparation of functional telechelic polymers, which can be further utilized to reinitiate NMP or to introduce the ruthenium complex. In the first part of this work, the polymerization kinetics are investigated by SEC, NMR spectroscopy, and complemented by mass spectrometry. The second part describes the isolation and characterization of a ruthenium-decorated poly(triarylamine), including a brief discussion of the ground state UV−vis absorption behavior and electrochemical features.

EXPERIMENTAL SECTION

Materials. $[Ru(dqp)(MeCN)_3][PF_6]_2$ and 2,6-di(quinolin-8-yl)-pyridin-4-ol were prepared as in the literature.[30]

*4-Methyl-N-p-tolyl-N-(4-vinylphenyl)aniline (**1**).* A flask was charged with 1-bromo-4-methylbenzene (11.411 g, 66.72 mmol), 4-vinylaniline (4.001 g, 33.56 mmol), sodium 2-methylpropan-2-olate (11.285 g, 133.71 mmol), 2,8,9-triisobutyl-2,5,8,9-tetraaza-1-phosphabicyclo[3.3.3]undecane (0.095 g, 0.27 mmol), bis-(dibenzylideneacetone)palladium(0) (0.154 g, 0.27 mmol), and dry toluene (300 mL). The reaction mixture was purged with N_2 for 5 min and heated to 85 °C for 10 h. The reaction mixture was allowed to cool to room temperature, filtered, and rinsed with dichloromethane, and the excess of solvent was removed under reduced pressure. The crude product was purified by flash column chromatography (silica, eluting with hexanes/dichloromethane) to yield a light-yellow solid (7.679 g, 76%). ^{1}H NMR (300 MHz, $CDCl_3$): δ 7.28 (d, J = 8.2 Hz, 2H), 7.08 (apparent d of AA′BB′, J = 8.4 Hz, 4H), 7.02 (apparent d of AA′BB′, J = 8.4 Hz, 4H), 7.00 (d, J = 8.2 Hz, 2H), 6.67 (dd, J = 17.6, 10.9 Hz, 1H), 5.63 (d, J = 17.6 Hz, 1H), 5.15 (d, J = 10.9 Hz, 1H), 2.34 (s, 6H). ^{13}C NMR (75 MHz, $CDCl_3$): δ 148.0, 145.3, 136.5, 132.7, 131.1, 130.0, 127.0, 124.8, 122.5, 111.7, 20.9. EI-MS m/z (M^+) calcd for $C_{22}H_{21}N$ 299; found 299.

*4-Fluoro-N-(4-fluorophenyl)-N-(4-vinylphenyl)aniline (**2**).* Using 4-vinylaniline (0.298 g, 2.5 mmol, 1 equiv), in toluene (50 mL). Yield 65%. ^{1}H NMR (400 MHz, $CDCl_3$): δ 7.31 (apparent d of AA′BB′, J = 8.6 Hz, 2H), 7.12−6.94 (m, 10 H), 6.68 (dd, J = 17.6, 10.9 Hz, 1H), 5.66 (d, J = 17.6, 1H), 5.18 (d, J = 10.9 Hz, 1H). ^{13}C NMR (100 MHz, $CDCl_3$): δ 160.3, 157.9, 147.7, 143.8 (2×), 136.2, 131.8, 127.3, 126.2 (2×), 122.5, 116.4, 116.2, 112.3, Anal. Calcd for $C_{20}H_{15}NF_2$: C, 78.16; H, 4.92; N, 4.56. Found: C, 77.55; H, 5.21; N, 4.64. EI-MS m/z (M^+) calcd for $C_{20}H_{15}NF_2$ 307; found 307.

*4-Methoxy-N-(4-methoxyphenyl)-N-(4-vinylphenyl)aniline (**3**).* Using 4-vinylaniline (0.298 g, 2.5 mmol, 1 equiv), in toluene (50 mL). Yield 33%. ^{1}H NMR (300 MHz, $CDCl_3$): δ 7.26 (apparent d of AA′BB′, J = 8.6 Hz, 2H), 7.08 (apparent d of AA′BB′, J = 8.9 Hz, 4H), 6.92 (apparent d of AA′BB′, J = 8.9 Hz, 2H), 6.86 (apparent d of AA′BB′, J = 8.6 Hz, 4H), 6.66 (dd, J = 17.6, 10.8 Hz, 1H), 5.61 (dd, J = 17.6, 1.0 Hz, 1H), 5.12 (dd, J = 10.8, 1.0 Hz, 1H), 3.82 (s, 6H). ^{13}C NMR (75 MHz, $CDCl_3$): δ 156.0, 148.6, 141.0, 136.5, 130.1, 127.0, 126.6, 120.6, 114.8, 111.2, 55.6. EI-MS m/z (M^+) calcd for $C_{22}H_{21}NO_2$ 331; found 331.

*[Ru(dqp)(dqpOH)][PF$_6$]$_2$ (**4**).* A flask was charged with $[Ru(dqp)(MeCN)_3][PF_6]_2$ (0.513 g, 0.484 mmol), 2,6-di(quinolin-8-yl)pyridin-4-ol (0.170 g, 0.487 mmol), and ethylene glycol (20 mL). The reaction mixture was heated to 120 °C under N_2 for 16 h. The reaction mixture was allowed to cool to room temperature, followed by dropwise addition into an aqueous solution of ammonium hexafluorophosphate. The solids were filtered off, washed with a slight amount of water, and redissolved in acetonitrile. The crude product was purified by column chromatography (silica, eluent acetonitrile/water/potassium nitrate 40:4:1), the streaking red band was collected, and the excess of solvent was removed under reduced pressure. Aqueous ammonium hexafluorophosphate was added, and the suspension extracted three times with dichloromethane. The solids were filtered off, washed with little water and diethyl ether, and dried under reduced pressure to yield a first crop (0.251 g). The combined organic layers were washed with water, and excess of solvent was removed under reduced pressure. The product was recrystallized from acetonitrile by vapor diffusion of diethyl ether to yield a second crop (0.097 g). Total yield (0.348 g, 67%). ^{1}H NMR (250 MHz, CD_3CN): δ 8.13 (t, J = 8.0 Hz, 1H), 8.12−7.99 (m, 8H), 7.85 (d, J = 8.1 Hz, 2H), 7.73−7.62 (m, 8H), 7.43 (t, J = 7.8 Hz, 2H), 7.42 (d, J = 7.8 Hz, 2H), 7.37 (s, 2H), 7.07 (dd, J = 8.3, 5.2 Hz, 2H), 7.03 (dd, J = 8.3, 5.2 Hz, 2H). ^{13}C NMR (CD_3CN, 63 MHz): δ 167.1, 159.6, 158.4, 157.9, 147.7, 147.6, 138.8, 138.5, 138.3, 133.9, 133.7, 133.0, 132.8, 131.5, 128.9, 127.8, 127.8, 127.7, 123.0, 122.8, 117.1. ESI-MS m/z ($[M-H-2PF_6]^+$) calcd for $C_{46}H_{29}N_6ORu$ 783.1453; found 783.1441.

Polymerization. *General Procedure for Small-Scale Polymerization Using MAA-SG1 ("Blocbuilder").* A stock solution of the initiator (18.3 mg) was prepared using toluene/anisole (9:1, 2.5 mL). A microwave vial was charged with the monomer and stock solution, sealed, and purged for 30 min with N_2, which was bubbled through a

dx.doi.org/10.1021/ma302631f | Macromolecules XXXX, XXX, XXX−XXX

mixture of toluene/anisole (9:1) before. The reaction mixture was heated to 115 °C for 13 h. The reaction mixture was allowed to cool to room temperature, diluted with toluene, and analyzed by SEC and NMR. The crude product was isolated by precipitation into ice-cold methanol (50 mL), filtered, washed with cold methanol and dried under reduced pressure. Remaining monomer was removed by size-exclusion chromatography on Biobeads to yield an off-white solid.

P1 (Table 1, entry 1) was prepared according to the general procedure using 4-methyl-*N*-*p*-tolyl-*N*-(4-vinylphenyl)aniline (**1**) (0.228 g, 0.762 mmol) and 0.38 mL of the stock solution of MAA-SG1 (2.78 mg, 7.29 μmol). Yield: 0.180 g.

P2 (Table 1, entry 2) was prepared according to the general procedure using 4-fluoro-*N*-(4-fluorophenyl)-*N*-(4-vinylphenyl)aniline (**2**) (0.240 g, 0.781 mmol) and 0.39 mL of the stock solution of MAA-SG1 (2.85 mg, 7.47 μmol). Yield: 0.150 g.

P3 (Table 1, entry 3) was prepared according to the general procedure using 4-methoxy-*N*-(4-methoxyphenyl)-*N*-(4-vinylphenyl)-aniline (**3**) (0.228 g, 0.688 mmol) and 0.34 mL of the stock solution of MAA-SG1 (0.251 mg, 0.658 μmol). Yield: 0.038 g.

P4 (Table 1, entry 4) was prepared according to the general procedure using styrene (0.121 g, 1.162 mmol) and 0.58 mL of the stock solution of MAA-SG1 (4.246 mg, 0.011 mmol). Product was analyzed but not isolated.

P5 (Table 1, entry 5). A microwave vial was charged with 4-methyl-*N*-*p*-tolyl-*N*-(4-vinylphenyl)aniline (**1**) (0.500 g, 1.67 mmol) and MAA-SG1 (0.064 g, 0.167 mmol) and sealed with a septum. Dry *N*,*N*-dimethylformamide (1.7 mL) was added via a syringe, and the mixture was purged for 1 h with N_2. The reaction mixture was heated to 115 °C, and samples were taken for SEC and NMR analysis. The polymer was precipitated into cold methanol, redissolved in dichloromethane, and further purified by size-exclusion chromatography on Biobeads (SX-3) for final NMR analysis.

General Procedure with CMSt-TIPNO. The reaction vessel, a sealable glass tube (1 mL) equipped with external overhead flushing with protective gas (see Supporting Information), was charged with 4-methyl-*N*-*p*-tolyl-*N*-(4-vinylphenyl)aniline (**1**), *N*-(*tert*-butyl)-*O*-(1-(4-(chloromethyl)phenyl)ethyl)-*N*-(2-methyl-1-phenylpropyl)-hydroxylamine (CMSt-TIPNO), and solvent. The reaction vessel was sealed, purged with N_2 for 20 min, and immersed in a preheated oil bath (120 °C). Samples were taken at given times for SEC and NMR analysis.

P6 (Table 1, entry 6) was prepared according to the general procedure using 4-methyl-*N*-*p*-tolyl-*N*-(4-vinylphenyl)aniline (**1**) (0.500 g, 1.67 mmol), CMSt-TIPNO (0.031 g, 0.083 mmol), and *N*,*N*-dimethylformamide (1.7 mL). The remaining reaction mixture was directly used for the postmodification with **4** (read below).

P7 (Table 1, entry 7) was prepared according to the general procedure using 4-methyl-*N*-*p*-tolyl-*N*-(4-vinylphenyl)aniline (**1**) (1.818 g, 6.07 mmol), CMSt-TIPNO (0.023 g, 0.061 mmol), and anisole (2.0 mL). The polymer was precipitated into cold methanol, redissolved in dichloromethane, and further purified by size-exclusion chromatography on Biobeads (SX-1). Reprecipitation of the polymer into methanol gave a white powder. Yield: 0.492 g.

Reinitiation of P6 was performed according to the general procedure using 4-methyl-*N*-p-tolyl-*N*-(4-vinylphenyl)aniline (**1**) (0.740 g, 2.46 mmol), **P6** (0.050 g, 2.45 μmol assuming M_n = 20 400 g/mol from poly(styrene) calibration of SEC), and anisole (2.5 mL). The final reaction solution was added dropwise to cold methanol and analyzed by SEC.

***In situ* modification of P6.** The reaction mixture of crude **P6** (read above) was allowed to cool to room temperature, followed by addition of **4** (0.098 g, 0.091 mmol), potassium carbonate (0.012 g, 0.087 mmol), and *N*,*N*-dimethylformamide (2 mL). The solution was purged for 20 min and heated to 60 °C for 4 days afterward. The reaction mixture was poured into aqueous ammonium hexafluorophosphate (100 mL); the formed precipitate was filtered, rinsed with water, and redissolved in dichloromethane. The dark red solution was washed with water and dried over sodium sulfate. The crude product was purified by column chromatography on silica eluting with dichloromethane/methanol (9:1). Unreacted **4** was recovered by increasing the polarity of the eluent (acetonitrile/water/potassium nitrate 40:4:1). The crude product was further purified by size-exclusion chromatography on Biobeads (SX-3) to yield **Ru−P6** as a reddish solid (0.040 g).

RESULTS AND DISCUSSION

Monomer Synthesis. The palladium-catalyzed Hartwig−Buchwald coupling of *p*-aminostyrene with 2 equiv of a para-substituted bromobenzene gave the substituted styrenic triarylamines (**1**−**3**) (Scheme 2).[31,32] The convenient isolation of the product by column chromatography facilitates the straightforward up-scaling, e.g., the preparation of **1** on a multigram scale (10 g) with 76% yield. The NMR spectra (see Supporting Information) are composed of the partially overlapping signals of the aromatic protons (7.3−6.8 ppm) and the well-resolved vinylic group at approximately 6.7, 5.7, and 5.2 ppm. The methyl groups appear as singlets at 2.34 ppm (**1**) and 3.82 ppm (**3**). However, the isolated yield of **3** was lower, and a significant photoinstability of **3** was noticed in solution under ambient conditions. When a sample is exposed to sun light, the quantitative conversion to a new species with the double molar mass is observed. The structural assignment of the photoproduct is provided in the Supporting Information and supported by NMR analysis. The ^{1}H NMR spectrum shows the typical chemical shifts and the coupling constant (J = 16.0 Hz) of a trans-alkene group adjacent to a CH group (see Supporting Information). In addition, an aliphatic methyl group appears as a doublet (J = 7.0 Hz) with a pronounced high-field shift (1.5 ppm). It is well-known that Lewis acids (e.g., protons or transition metals) promote the dimerization of styrenes, but the formation of excimers or the presence of oxygen also lead to similar photoreactions, as observed in zeolites.[33] However, the conversion of the methyl- and fluoro-substituted triarylamines required exposure to UV light for an extended time. The photochemical behavior of the monomers suggests that the dimerization via a radical cation is likely: no cyclic [2 + 2] photoproducts or polymeric side products were found, and the reactivity increases (F < Me ≪ OMe) with decreasing oxidation potentials (see Electrochemistry).

Polymerization with Blocbuilder. The nitroxide-mediated polymerization of **1**−**3** was first investigated using the MAA-SG1 initiator. The reactions were performed applying typical conditions of NMP (Scheme 2),[3] i.e., a monomer/initiator ratio of 100:1 in 2 M solutions in toluene/anisole (9:1) at 115 °C (Table 1, entries 1−4) for 13 h. The SEC analysis of **P1**−**P3** confirmed the successful polymerization, although the polymers display a broad range of molar masses and significantly larger PDI values than expected. In particular, the electron-rich monomer **3** revealed the loss of control during polymerization. For comparison, the polymerization of styrene under identical conditions was investigated (entry 4). The analysis of **P4** showed similar conversion (66% by ^{1}H NMR), but a somewhat larger molar mass (M_n = 8470 g/mol) and PDI value (1.26) than anticipated. The nonideal behavior of these initial experiments are attributed to the small scale (0.2 mL), e.g., by evaporation of solvent or termination reactions by residual oxygen. Hence, the real radical concentrations would differ significantly from the initial values and thereby affect the apparent rate of conversion, the obtained molar masses, and PDI values. However, the absolute values of the SEC analysis should also be taken with care due to the unknown hydrodynamic volume of the polymers. In order to gain a detailed insight into the course of the reaction in the early stage,

dx.doi.org/10.1021/ma302631f | *Macromolecules* XXXX, XXX, XXX−XXX

Scheme 2. Synthesis and Polymerization of Triarylamines 1−3[a]

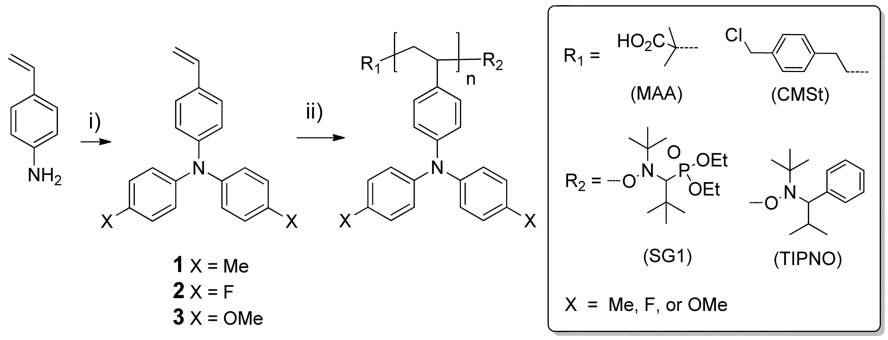

[a]Reagents and conditions: (i) 2 equiv of *para*-substituted bromobenzene, Pd^0, phosphine ligand, NaO^tBu, toluene, N_2, 85 °C, 10 h; (ii) see Table 1.

Table 1. Polymerization of 1−3 at 115 °C

polymer	monomer	initiator	M/I	solvent	conc [M]	time [h]	conv[a] [%]	M_n[b] [g/mol]	PDI
P1	**1**	MAA-SG1	100	toluene/anisole (9:1)	2	13	66	8060 (27)[c]	1.51[c]
P2	**2**						>99	26200 (85)[c]	1.27[c]
P3	**3**						76	231000 (697)[c]	1.96[c]
P4	styrene						66	8470 (81)[c]	1.26[c]
P5	**1**	MAA-SG1	10	DMF	1	1.2	74	1700 (5.7)[c]	1.19[c]
						2	81	2230 (5.4)[c]	1.24[c]
						3	86	2600 (8.6)[c]	1.28[c]
P6	**1**	CMSt-TIPNO	20	DMF	1	22	73	3840 (9.5)[d]	1.13[d]
P7	**1**	CMSt-TIPNO	60	anisole	3	20	77	10550 (35)[d]	1.17[d]

[a]Determined from ^{1}H NMR data. [b]Apparent molar mass by PS calibration; the degree of polymerization is given in parentheses. [c]SEC in DMAc + 0.21% LiCl with PS calibration. [d]SEC in $CHCl_3$, isopropanol, triethylamine (94:2:4) with PS calibration.

we followed the conversion of **1** with a lower monomer/initiator ratio (10:1). In view of a subsequent *in situ* postpolymerization modification, the solvent was changed (DMF) to promote the solubility of a suitable Ru^{II} complex (see below). Samples of **P5** were taken hourly and analyzed by SEC and ^{1}H NMR spectroscopy (Figure 1). The controlled polymerization is reflected by low PDI values (<1.3), but the fast conversion precluded a more detailed kinetic analysis. The small shoulder (t = 22.3 min) is attributed to side reactions before the first sampling because this contribution remains unchanged in latter samples. At this stage, the somewhat larger PDI values at later times may also arise from chain−chain coupling reactions. The polymerization was stopped, and the product purified by preparative SEC. The ^{1}H NMR spectrum of **P5** shows the backbone signals of the polymer (1.4−2.4 ppm) and the characteristic resonances of the SG1 end group. In comparison to the initiator, the typical signal broadening within polymers is observed, whereas the different magnetic environment results in a high-field shift of the end group's signals. In addition, the new chiral centers of the backbone lead to diastereomers, which cause a more complex set of signals of the SG1 group. In this regard, the phosphorus-decoupled spectrum can be finally utilized to unambiguously assign the different P-containing species (see Figure 1, at 3.2−3.4 ppm).

Polymerization with a TIPNO-Based Initiator. The polymerization of **1** was investigated next using CMSt-TIPNO as initiator in DMF to assist the *in situ* modification with a ruthenium complex (see below) and in anisole for enhanced solubility. The course of the reaction was followed by SEC and ^{1}H NMR spectroscopy (Figure 2). The conversion was determined by ^{1}H NMR from the disappearance of the vinyl group with respect to the aromatic protons. In addition, the characteristic signals of the initiator, i.e., the CMSt and the TIPNO moiety, can be used to analyze the reaction mixtures. However, the ^{1}H NMR spectrum of the initiator is complicated due to diastereomers (see Figure 2, t = 0 min), which can be identified by 2D data in agreement with the literature data (see Supporting Information).[34] The two CH_2 signals of the diastereomeric chloromethyl groups appear as singlets at 4.58 and 4.61 ppm. The TIPNO fragment displays two sets in the aliphatic region, with a pronounced high-field shift of one CH_3 group (0.22 ppm). Upon incorporation into the polymer (**P6**), both fragments exhibit a significant line broadening and a small but distinct high-field shift (0.1−0.2 ppm), which is attributed to the different magnetic environment of the triarylamine unit (Figure 2). The initiation stage can be estimated by the changes of the characteristic signals of the end groups, but the exact and reliable determination of the initiator efficiency suffers from the low intensity, overlapping signals, and the formation of diastereomers. However, the consumption of the initiator occurs within ∼75 min, followed by the formation of transient oligomeric species, as judged from the sharp signals around 4.50 ppm. At later times, the broad signals of the polymer evolve around 4.40 ppm. Noteworthy, the remaining minor contribution of the initiator suggests incomplete initiation.

The SEC analysis of **P6** provides a more detailed insight into the polymerization (Figure 2). During the initial stage (<2 h), the transient oligomeric species (10.5−11.0 min) are resolved due to the sufficiently large molar mass difference. The separation between each species agrees well with the theoretical value (see Supporting Information), although a strict comparison would require a precise calibration. At later times, the polymer chains grow and the curves shift to shorter elution volumes. In line with previous experimental results, a

dx.doi.org/10.1021/ma302631f | *Macromolecules* XXXX, XXX, XXX−XXX

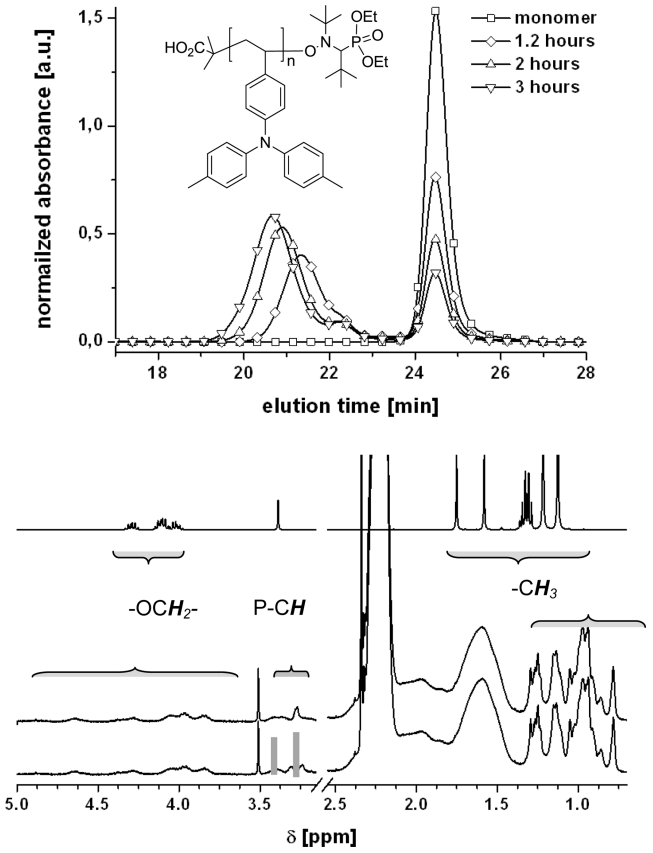

Figure 1. (top) Normalized SEC traces of **P5** at given times and ^{1}H NMR spectra ($CDCl_3$, 400 MHz, aliphatic region): (3rd from bottom) MAA-SG1 with P-decoupling, (2nd from bottom) **P5** with P-decoupling, and (bottom) without P-decoupling, including proton assignment of the SG1 moiety with typical regions (in brackets) and effect of P-decoupling (vertical lines) of the PCH group (around 3.3 ppm).

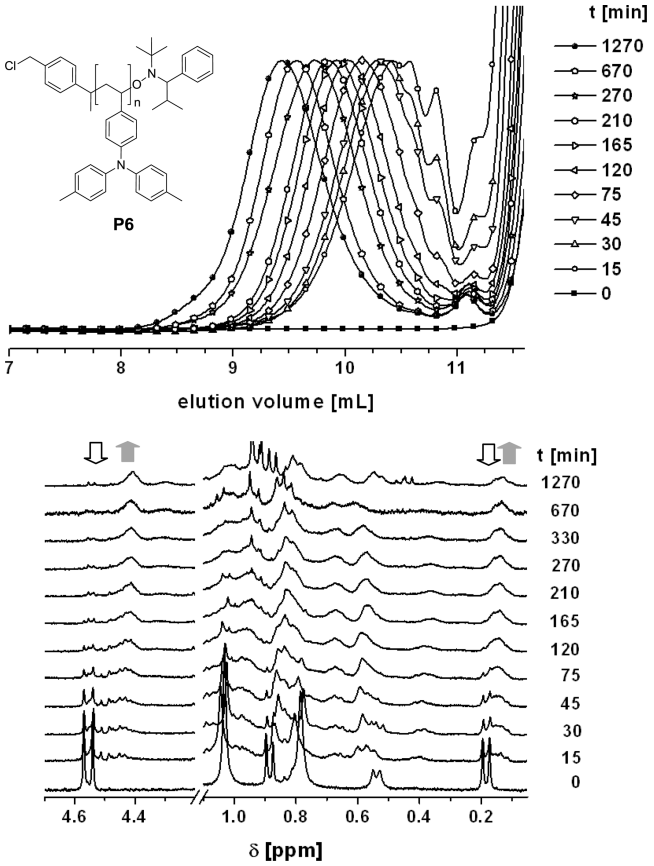

Figure 2. Polymerization of **1** in DMF: (top) normalized SEC traces (UV detection at 342 nm) of **P6** after given times, and (bottom) ^{1}H NMR spectra (300 MHz, $CDCl_3$, aliphatic region) of crude **P6** after given times; the changes of the CMSt group (4.55 ppm) and TIPNO (0.18 ppm) are indicated by arrows.

low-molar-mass species is observed throughout the polymerization. The amount seems invariant because no changes are observed for the latter samples, whereas the relative contribution decreases for the first samples due to the normalization of the UV signal. These findings are in line with the results of the NMR analysis. The kinetic analysis of **P6** shows a linear increase of the molar mass with low PDI values (<1.2) (Figure 3). The second important feature of the polymerization is the steady conversion of monomer over time. The linear relationship between $\ln(M_0/M_t)$ and time is predicted in the ideal case of (1) a fast initiation vs propagation rate, (2) the absence of terminating reactions, and (3) propagation rates independent of the chain length. However, if these assumptions are not met, a diverse kinetic behavior is observed instead, as discussed in a recent review on the kinetics of NMP.[35] The experimental data of **P6** show a pronounced deviation from the ideal behavior, i.e., a significant decrease of the propagation rate during the course of the reaction. The common explanation of such a behavior is provided by the persistent radical effect (PRE),[36] arising from termination reactions of the polymer radicals and the buildup of free nitroxide. Analytical solutions of the rate laws were derived to account for the PRE, i.e., plotting the data vs $t^{2/3}$ instead.[36,37] Although a linear relationship can be reasoned up to 2 h, later samples show a slower growth of the chains. This finding suggests further rate-retarding processes, which are ascribed to chain-length-dependent effects, the penultimate effect, etc.[35] However, a more detailed kinetic analysis, i.e., the determination of the individual rate constants of initiation, propagation or termination steps, is beyond the scope of this study. More importantly, the slower propagation at later times seems to compensate for the relatively long initiation period, as judged from the decrease of the apparent PDI values. Hence, the faster growth of late-initiated chains narrows the polymers' polydispersity during the reaction. Finally, termination reactions seem to play only a minor role, as judged from the low PDI value at maximum conversion (up to 75%). A similar behavior was found for **P7** in anisole with a 3-fold M/I ratio, which gave a polymer with ~3-fold molar mass (Figure 3).

Mass Spectrometry. The polymerization products were further investigated by mass spectrometry (Figure 4). A cutoff of ions with molar masses below 780 m/z was applied to increase the signal intensity in the high molar mass region. The MALDI spectrum shows a major distribution with the characteristic molar mass of the repeating unit (300 m/z), reaching up to 7000 m/z. However, the ion mass differs from the proposed dormant species, which could originate from the known decomposition of nitroxides.[38] The fragmentation of TIPNO-based polymers is reported to depend on the exact ionization conditions (matrix, additives, laser intensity, etc.) to give both N−C scission products, the related H-abstraction products,[39] and/or the main chain scission products,[40] in particular at higher laser intensities.[41] However, none of such

dx.doi.org/10.1021/ma302631f | *Macromolecules* XXXX, XXX, XXX−XXX

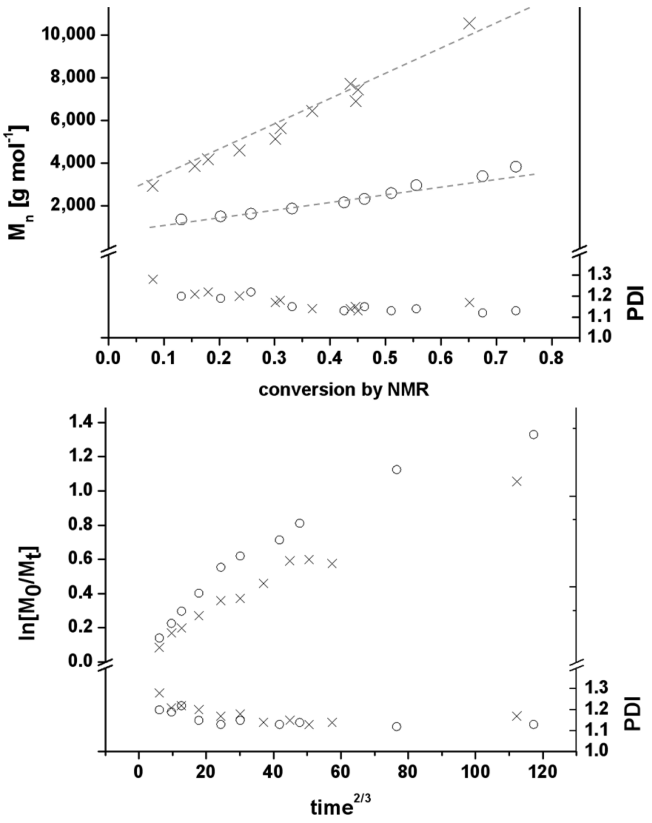

Figure 3. Kinetic analysis of **P6** (crosses) using M/I 20:1, 1 M in DMF, and **P7** (circles) using M/I 60:1, 3 M in anisole. M_n, M_w, and PDI values were determined by SEC ($CHCl_3$, isopropanol, triethylamine 94:2:4), conversion determined from ^1H NMR data. See Supporting Information for linear plot of $\ln(M_0/M_t)$ vs time.

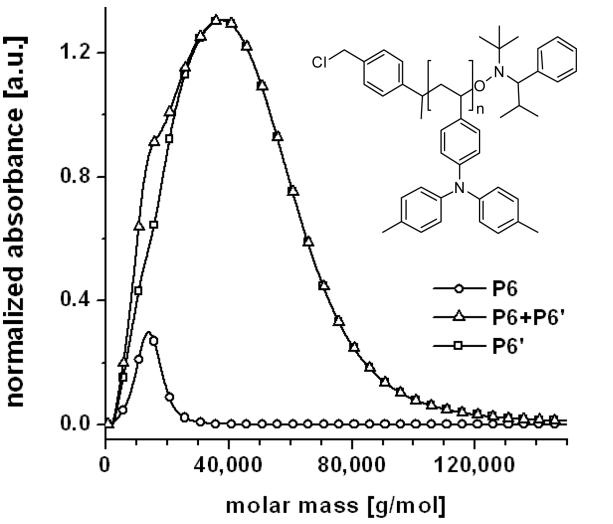

Figure 5. Normalized SEC-UV traces of the reinitiation study of **P6**: macroinitiator (**P6**), reaction product (**P6** + **P6′**), and deconvolved trace of the chain-extended polymer (**P6′**).

species can be correlated with the experimental data. A plausible explanation for this unusual behavior is the absorption of the laser light (355 nm) by the triarylamine chromophore, which may initiate photoreactions that compete with the conventional desorption process.[42] The MS/MS fragmentation of the ions leads primarily to cleavage of the backbone and formation of fragments with low molar masses, which are assigned to one or two triarylamine units with up to three methylene groups (see Supporting Information), respectively. If the site of fragmentation is close to the chain terminus, the resulting ions contain also the initiator moiety. In case of the **P6**, the characteristic isotope pattern of CMSt with one or two repeating units is identified (see Figure 4 and Supporting Information).

The ESI-MS data of the polymer show a strong discrimination of high molar masses in comparison to the MALDI technique (Figure 4). The main distributions are singly charged and display the typical mass difference of the repeating unit, but none of the species belong to the intact polymer chain. However, the thermally labile nitroxide may cleave off during the ESI process to form secondary products. A more detailed analysis of the exact mechanism of ionization and fragmentation is beyond the scope of this study and subject of a forthcoming publication applying complementary state-of-the-art MS techniques.[43] However, the controlled nature of the polymerization and the NMR analysis indicates the presence of the nitroxide, whereas the MS and MS/MS data support only the presence of the CMSt group.

Reinitiation. The polymer **P6** was tested to reinitiate the polymerization of **1** using the general procedure. A monomer-to-initiator ratio of 1000:1 was chosen to compensate for the low propagation rates. After purification, the SEC analysis

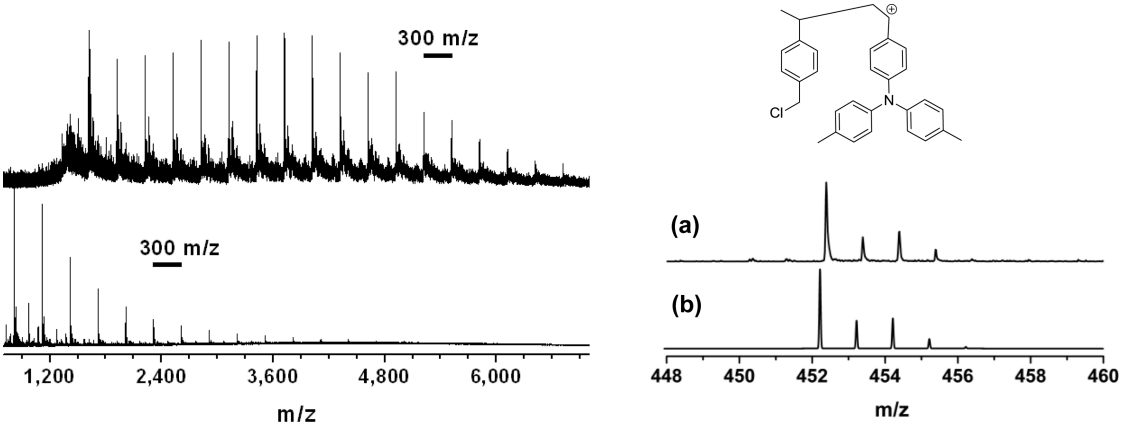

Figure 4. Mass spectrometry data of **P6**: MALDI-ToF (top left, matrix: dithranol) and ESI-ToF (bottom left), and expansion (right) of a representative fragment ion from the MALDI-ToF spectrum (a), isotope simulation (b), and the proposed structure.

dx.doi.org/10.1021/ma302631f | *Macromolecules* XXXX, XXX, XXX–XXX

shows a bimodal distribution, which can be assigned to the unreacted macroinitiator (**P6**) and the chain-extended polymer (**P6′**) (Figure 5). The efficiency of the reinitiation can be estimated from the UV absorption data plotted vs the molar mass based on the following simplifications: (1) the degree of polymerization is proportional to the apparent molar mass using PS calibration, and (2) the number of repeating units is proportional to the absorbance. Hence, the ratio of incorporated monomer units in the **P6′** vs macroinitiator is ca. 95:5, as derived from the deconvolved peak areas (Figure 5). The controlled growth of the polymer is an indirect argument for the presence of the nitroxide group in **P6**, in line with the SEC and NMR data (see above).

Postpolymerization Modification with Ruthenium. The defined introduction of a ruthenium complex was investigated via a nucleophilic substitution reaction of the CMSt group of **P6** (Scheme 3). The hydroxyl-functionalized ruthenium complex (**4**) was readily prepared by ligand substitution reaction of $[Ru(dqp)(MeCN)_3]^{2+}$ in analogy to a literature procedure.[30] The modification was performed *in situ* at 60 °C in the crude polymer solution in order to minimize the extent of possible side reactions of the CMSt group during isolation. Noteworthy, the concurrent growth of the chains is negligible due to the substantially lower reaction temperature. The product was readily purified by column chromatography on silica because the high polarity of the cationic ruthenium complex enables the removal of excess of nonfunctionalized polymer and the recovery of **4**. A final preparative size-exclusion chromatography step was performed to separate any remaining nonfunctionalized polymer. The purified product was analyzed by SEC, 2D NMR spectroscopy, and mass spectrometry.

Scheme 3. Postpolymerization Modification of P6[a]

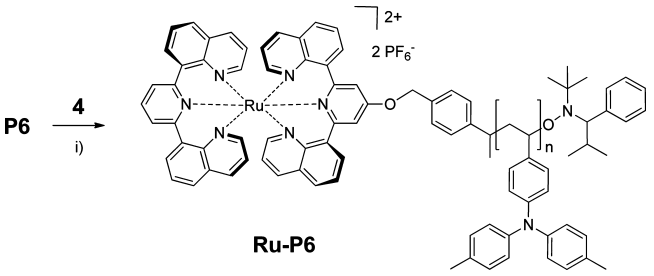

[a]Reagents and conditions: (i) K_2CO_3, DMF, 60 °C, N_2.

The 3D SEC plot of **Ru−P6** is shown in Figure 6. The UV trace is composed of the very strong absorption from the triarylamine units below 350 nm and the typical MLCT transition of the ruthenium fragment around 500 nm. Interestingly, the elution volume is slightly larger than for the nonfunctionalized precursor polymer (+0.1 mL, see Supporting Information). The apparent smaller hydrodynamic volume can by reasoned by a more compact conformation of **Ru−P6** compared to **P6** or by retention due to surface interactions of the charged species. However, the size-exclusion effect is evident from the comparison with the precursor complex **4**, which elutes significantly later (+0.8 mL, see Supporting Information). The ^{1}H NMR spectrum of the purified sample shows the strong signals of the triarylamine units between 6.3 and 7.0 ppm and the well-resolved peaks of the ruthenium fragment above 7.0 ppm. The methylene protons of the linker unit can be unambiguously identified by the phase-sensitive C−H correlation technique (Figure 7). However, the cross-peaks of the TIPNO group in the aliphatic region overlap with the strong backbone signals and preclude a definite assignment. The comparison of the aromatic signals of the ruthenium and triarylamine moieties gives a numerical ratio of 1:14 for **Ru−P6**, in good agreement with the precursor polymer.

The MALDI-ToF measurements required a cutoff to detect any higher molar mass components (Figure 8). The major series of the singly charged polymer shows the broad isotope

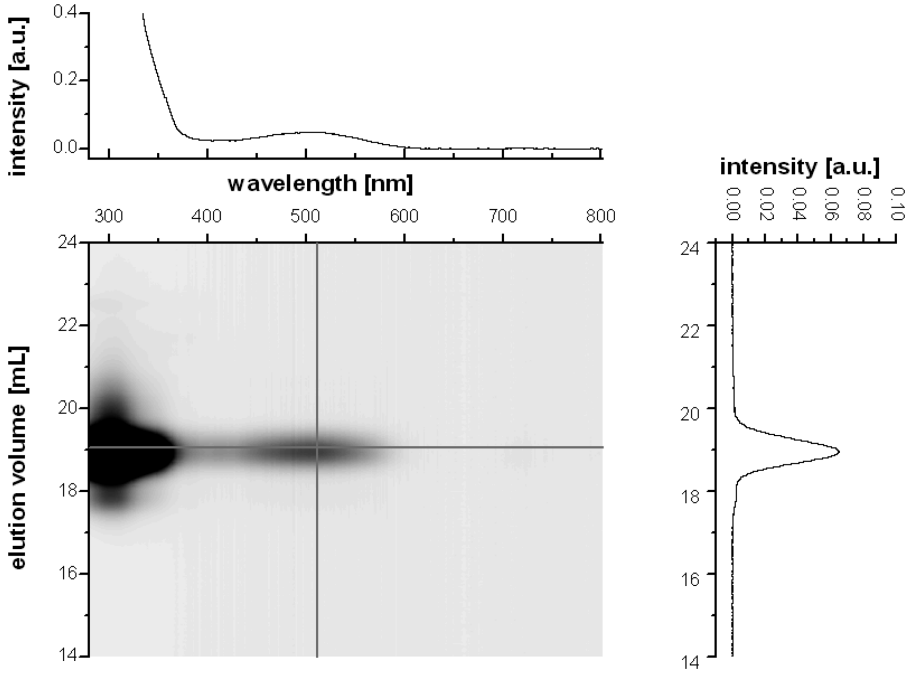

Figure 6. 3D SEC data (wavelength vs elution time, DMAc + 0.08% NH_4PF_6) of **Ru−P6** with projections: (top) UV trace at 19.1 mL; (right) chromatogram at 515 nm in au.

dx.doi.org/10.1021/ma302631f | *Macromolecules* XXXX, XXX, XXX−XXX

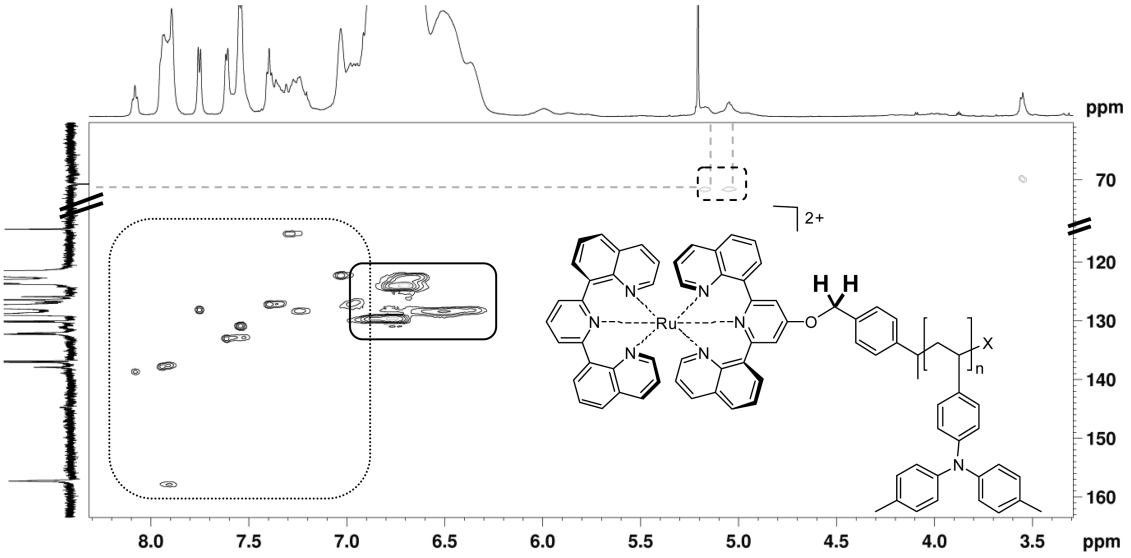

Figure 7. Expanded HSQC spectrum of **Ru−P6** with assignment of characteristic cross-peaks, assigned to the Ru fragment (dotted), the poly(triarylamine) (solid), and the CH_2−group of the linker (dashed).

pattern of ruthenium, which can be assigned to the formula [**Ru−P6** + PF_6^-−H^+] without the TIPNO fragment. The MS/MS investigation showed the dominant C−O cleavage (783 m/z): the major signal without using the cutoff, the elimination of HPF_6 (−146 m/z), and two nonidentified ruthenium-containing species (see the Supporting Information). However, a more detailed analysis was precluded by the low signal intensity, which may arise from the challenging desorption of the doubly charged ruthenium species and competitive absorption of the laser light, which explains also the pronounced C−O scission. Noteworthy, a higher laser power only leads to more pronounced fragmentation (see above).

Hence, the softer ESI-ToF technique may provide additional structural information on the ionic species. The spectrum of **Ru−P6** consists of several high molar mass species (Figure 8), in which the main series can be assigned to doubly and triply charged [**Ru−P6**−H^+] with fitting isotope pattern (Figure 8). However, no intact **Ru−P6** with the attached TIPNO group was detected. Furthermore, two minor unidentified species were found with +15 and +31 m/z relative to the major series. The MS/MS analysis of the major series provides additional support for the proposed structure (see the Supporting Information): First, the ruthenium-containing fragments can be easily identified by their characteristic isotope pattern. The most intense signal originates from the cleavage of the complex (783 m/z), whereas the fragmentation along the polymer backbone gives significantly less intense signals. The organic fragment (583 m/z) can be assigned to the allyl cation bearing two triarylamine units, which can be explained by main chain scission. In addition, a characteristic series of organic fragments containing the styrene unit with multiple repeating units are observed. This fragmentation behavior can be reasoned by assuming the concurrent scission along the backbone upon cleavage of the ruthenium moiety. In conclusion, the MS and MS/MS data support the presented structure of **Ru−P6**, but no indication of the nitroxide moiety was found. However, thermal cleavage of the labile nitroxide group during the ESI process cannot be ruled out.

Electrochemical and Optical Properties. The redox properties of the homopolymers **P1−P3** and **Ru−P6** were investigated by cyclic voltammetry (CV) and differential pulse voltammetry (DPV). The potentials were referenced vs the ferrocene/ferrocenium couple (Table 2). First, the three substituted polymers show an oxidation process formally assigned to the oxidation of the triarylamine moiety. The electronic influence of the substituents (F, Me, OMe) is reflected by a shift in potential of the redox couple. The oxidation of **P1** occurs around +0.41 V, whereas the electron-withdrawing fluoro substituents of **P2** cause a shift to higher potential (+0.58 V), while the electron-releasing methoxy substituents of **P3** enable the oxidation already at lower potential (+0.26 V). The prototypical $[Ru(dqp)_2]^{2+}$ complex is oxidized at +0.63 V under similar conditions. With these data in hand, it is possible to calculate the thermodynamic driving force of electron transfer from the homopolymer to a Ru^{III} center, which is generated after oxidative quenching of the excited state. The calculated values increase in the order **P2** < **P1** < **P3** with driving forces of −0.05, −0.22, and −0.37 eV, respectively. The broad waves of the homopolymers further indicate additional processes beyond diffusion and the mere electrode surface kinetics. For example, the hypothetical oxidation of one triarylamine unit will affect the nearby units, leading to higher potentials required for their subsequent oxidation. In addition, further phenomena may contribute to the electrochemical response of the polymers, e.g., conformational changes of the polymer backbone to accommodate the charges and the associated counterions, aggregation phenomena upon (multiple) oxidation, or charge migration among the redox-active units on the time scale of the experiments. Homopolymer **P1** was also investigated in dichloromethane, which caused an appreciable cathodic shift by ∼60 mV. A similar behavior was found for the **Ru−P6**, which maintained the individual features of the components. First, the ligand-based reduction is found at −1.73 V, whereas the intense but broad wave around +0.37 V can be attributed to the oxidation of the triarylamine units. Upon re-reduction, the $Ru^{III/II}$ redox process becomes visible, followed by the reversible re-reduction of the polymer. Because of overlapping peaks, the potentials were extracted from the DPV data and agree very well the data of the individual components. The oxidation potential of the ruthenium center

dx.doi.org/10.1021/ma302631f | *Macromolecules* XXXX, XXX, XXX−XXX

Table 2. UV−Vis Absorption Data and Electrochemical Data vs Fc/Fc^+

compound	λ_{abs}[a] [nm]	E_{red} [V] (dqp/dqp$^{\bullet-}$)	E_{ox} [V] (TARA$^{\bullet+}$/TARA)	E_{ox} [V] (Ru^{III}/Ru^{II})	ΔG [eV] vs Ru^{III}/Ru^{II}
$[Ru(dqp)_2]^{2+}$ [b]	n.d.	−1.73		+0.63	0
P1[b]	302		+0.41		−0.22
P2[b]	294		+0.58		−0.05
P3[b]	299		+0.26		−0.37
P1[c]	n.d.		+0.35 (0.22)[d]		−0.28
Ru−P6[c]	302, 502	−1.73 (0.10)[d]	+0.37[e]	+0.63[e]	−0.26[e]

[a]In DMAc. [b]In DMF. [c]In dichloromethane. [d]Peak split (ΔE_p) in V. [e]From DPV data.

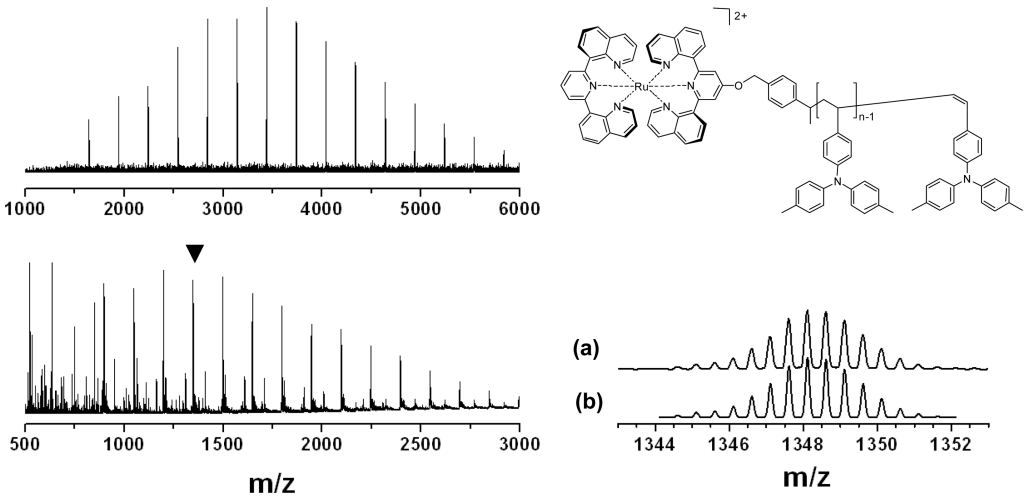

Figure 8. Mass spectrometry data of **Ru−P6**: MALDI-ToF (top left, matrix: dithranol), ESI-ToF (bottom left), and expansion (right) of a representative specimen (▼) from the ESI-ToF spectrum (a), isotope simulation (b), and the proposed structure.

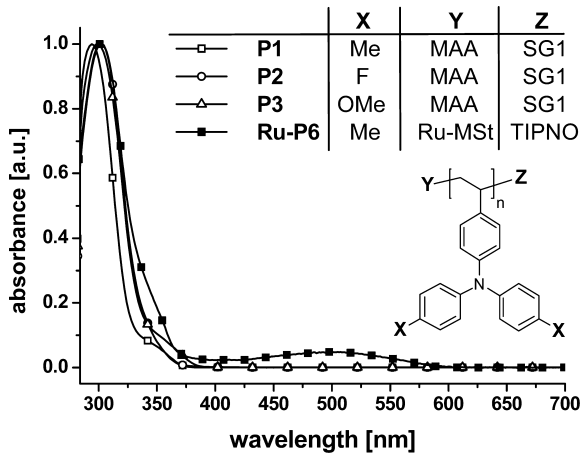

Figure 9. UV−vis absorption spectra of **P1−P3** and **Ru−P6** (in DMAc).

matches the value of the model complex in DMF. Hence, all homopolymers can act as an electron donor for the Ru^{III} center with adjustable driving force for the charge-injection step.

The UV−vis absorption spectra (Figure 9) of the homopolymers show a strong transition in the UV region centered around 300 nm. In case of **P2** and **P3**, a shoulder at higher wavelength is observed up to 380 nm. The **Ru−P6** displays the preserved optical features of the individual components: the triarylamine units dominate in the UV region, whereas the typical MLCT transition of the ruthenium complex is observed in the visible region (ca. 500 nm).

CONCLUSION

A redox-active architecture was synthesized by polymerization and subsequent modification with a photoactive ruthenium complex. Three styrenic triarylamine monomers were readily prepared by a one-pot procedure, including electron-withdrawing and -releasing substituents (**1−3**). Next, the nitroxide-mediated polymerization was investigated by SEC, NMR spectroscopy, and mass spectrometry. A kinetic analysis was performed for **1** to elucidate the scope of this approach toward telechelic redox-active architectures. Under typical NMP conditions, the initiation is completed within the first hour, and the polymer chain grows in a controlled fashion up to 75% conversion with low PDI values (<1.2). Noteworthy, the apparent polymerization rate decreases considerably during the reaction, beyond the anticipated influence of the persistent radical effect ($t^{2/3}$ plot). However, this effect compensates for the long initiation period. Both end groups of the telechelic redox-active polymer were successfully utilized: (a) to reinitiate the polymerization and (b) in the postmodification with a ruthenium complex via nucleophilic substitution. The homopolymers (**P1−P3**) and the **Ru−P6** were further investigated by UV−vis absorption spectroscopy and electrochemistry. The absorption spectra of the polymers are composed of the strong transitions in the UV region (<370 nm) of the triarylamine subunits and the typical MLCT of the ruthenium complex (~500 nm). The oxidation of the homopolymers occurs at less oxidizing potentials with respect to the $Ru(dqp)_2^{2+}$ and obeys the electronic influence of the substituents. The related **Ru−P6** shows a similar behavior with a driving force of electron transfer of ~260 mV. Hence, all homopolymers can act as electron donors to the Ru^{III} center (driving force of 0.05−0.22 eV). In

dx.doi.org/10.1021/ma302631f | Macromolecules XXXX, XXX, XXX−XXX

conclusion, the NMP of styrenic triarylamines represents a versatile route to assemble well-defined redox-active polymers, due to the following aspects: (a) the facile synthesis and isolation of the redox-tuned monomers, (b) the availability of functional initiators to yield telechelic linear polymers, (c) the successful reinitiation to access future block copolymers, and (d) the possibility to introduce a photoredox-active unit via postpolymerization manipulation. Hence, more sophisticated architectures with well-defined structure can be efficiently prepared, e.g., by connecting the complementary redox chain to the ruthenium center or by construction of redox-active segments utilizing block copolymers. In addition, the in-depth characterization of the photophysical and redox processes is expected to provide the ground to design the next generations of energy conversion systems.

■ ASSOCIATED CONTENT

Ⓢ Supporting Information

Additional instrumental details and analytical data of **1**−**4**, **P6**, and **Ru**−**P6** (NMR, MS, MS/MS, and SEC) provided for completion. This material is available free of charge via the Internet at http://pubs.acs.org.

■ AUTHOR INFORMATION

Corresponding Author

*E-mail: michael.jager.iomc@uni-jena.de (M.J.); ulrich.schubert@uni-jena.de (U.S.S.).

Author Contributions

The manuscript was written through contributions of all authors. All authors have given approval to the final version of the manuscript.

Notes

The authors declare no competing financial interest.

■ ACKNOWLEDGMENTS

M.J. is grateful for financial support of the Carl-Zeiss-Stiftung. We also thank Dr. Grit Festag for assistance with SEC measurements and Dr. Christine Weber for valuable discussion during the preparation of this manuscript.

■ ABBREVIATIONS

DMAc, *N*,*N*-dimethylacetamide; DMF, *N*,*N*-dimethylformamide.

■ REFERENCES

(1) Moad, G.; Chen, M.; Häussler, M.; Postma, A.; Rizzardo, E.; Thang, S. H. *Polym. Chem.* **2011**, *2*, 492.
(2) Braunecker, W. A.; Matyjaszewski, K. *Prog. Polym. Sci.* **2007**, *32*, 93.
(3) Hawker, C. J.; Bosman, A. W.; Harth, E. *Chem. Rev.* **2001**, *101*, 3661.
(4) Cheng, Y.-J.; Yang, S.-H.; Hsu, C.-S. *Chem. Rev.* **2009**, *109*, 5868.
(5) Guenes, S.; Neugebauer, H.; Sariciftci, N. S. *Chem. Rev.* **2007**, *107*, 1324.
(6) Hoppe, H.; Sariciftci, N. S. *J. Mater. Res.* **2004**, *19*, 1924.
(7) Thompson, B. C.; Frechet, J. M. J. *Angew. Chem., Int. Ed.* **2008**, *47*, 58.
(8) Nishide, H.; Oyaizu, K. *Science* **2008**, *319*, 737.
(9) Janoschka, T.; Hager, M. D.; Schubert, U. S. *Adv. Mater.* **2012**, *24*, 6397.
(10) Paddon-Row, M. N. In *Electron Transfer in Chemistry*; Wiley-VCH Verlag GmbH: Berlin, 2008; p 178.
(11) Behl, M.; Hattemer, E.; Brehmer, M.; Zentel, R. *Macromol. Chem. Phys.* **2002**, *203*, 503.
(12) Barea, E. M.; Garcia-Belmonte, G.; Sommer, M.; Hüttner, S.; Bolink, H. J.; Thelakkat, M. *Thin Solid Films* **2010**, *518*, 3351.
(13) Zorn, M.; Weber, S. A. L.; Tahir, M. N.; Tremel, W.; Butt, H.-J.; Berger, R.; Zentel, R. *Nano Lett.* **2010**, *10*, 2812.
(14) Yurchenko, O.; Freytag, D.; zur Borg, L.; Zentel, R.; Heinze, J.; Ludwigs, S. *J. Phys. Chem. B* **2011**, *116*, 30.
(15) Kwak, J.; Bae, W. K.; Zorn, M.; Woo, H.; Yoon, H.; Lim, J.; Kang, S. W.; Weber, S.; Butt, H.-J.; Zentel, R.; Lee, S.; Char, K.; Lee, C. *Adv. Mater.* **2009**, *21*, 5022.
(16) Zorn, M.; Zentel, R. *Macromol. Rapid Commun.* **2008**, *29*, 922.
(17) Sommer, M.; Lindner, S. M.; Thelakkat, M. *Adv. Funct. Mater.* **2007**, *17*, 1493.
(18) Tasdelen, M. A.; Kahveci, M. U.; Yagci, Y. *Prog. Polym. Sci.* **2011**, *36*, 455.
(19) Trimaille, T.; Mabrouk, K.; Monnier, V.; Charles, L.; Bertin, D.; Gigmes, D. *Macromolecules* **2010**, *43*, 4864.
(20) Juris, A.; Balzani, V.; Barigelletti, F.; Campagna, S.; Belser, P.; von Zelewsky, A. *Coord. Chem. Rev.* **1988**, *84*, 85.
(21) Campagna, S.; Puntoriero, F.; Nastasi, F.; Bergamini, G.; Balzani, V. In *Photochemistry and Photophysics of Coordination Compounds I*; Balzani, V. C. S., Ed.; Springer: Berlin, 2007; Vol. *280*, p 117.
(22) Gust, D.; Moore, T. A.; Moore, A. L. In *Electron Transfer in Chemistry*; Wiley-VCH Verlag GmbH: Berlin, 2008; p 272.
(23) Scandola, F.; Chiorboli, C.; Indelli, M. T.; Rampi, M. A. In *Electron Transfer in Chemistry*; Wiley-VCH Verlag GmbH: Berlin, 2008; p 337.
(24) Happ, B.; Winter, A.; Hager, M. D.; Schubert, U. S. *Chem. Soc. Rev.* **2012**, *41*, 2222.
(25) Huynh, M. H. V.; Dattelbaum, D. M.; Meyer, T. J. *Coord. Chem. Rev.* **2005**, *249*, 457.
(26) Morisaki, Y.; Chujo, Y. In *Conjugated Polymer Synthesis*; Wiley-VCH Verlag GmbH & Co. KGaA: Berlin, 2010; p 133.
(27) Morisaki, Y.; Ueno, S.; Saeki, A.; Asano, A.; Seki, S.; Chujo, Y. *Chem.—Eur. J.* **2012**, *18*, 4216.
(28) Abrahamsson, M.; Jäger, M.; Österman, T.; Eriksson, L.; Persson, P.; Becker, H.-C.; Johansson, O.; Hammarström, L. *J. Am. Chem. Soc.* **2006**, *128*, 12616.
(29) Abrahamsson, M.; Jäger, M.; Kumar, R. J.; Österman, T.; Persson, P.; Becker, H.-C.; Johansson, O.; Hammarström, L. *J. Am. Chem. Soc.* **2008**, *130*, 15533.
(30) Jäger, M.; Kumar, R. J.; Görls, H.; Bergquist, J.; Johansson, O. *Inorg. Chem.* **2009**, *48*, 3228.
(31) Nandakumar, M. V.; Verkade, J. G. *Tetrahedron* **2005**, *61*, 9775.
(32) Nandakumar, M. V.; Verkade, J. G. *Angew. Chem., Int. Ed.* **2005**, *44*, 3115.
(33) Matsubara, C.; Kojima, M. *Res. Chem. Intermed.* **2001**, *27*, 975.
(34) Britze, A.; Moellmann, V.; Grundmeier, G.; Luftmann, H.; Kuckling, D. *Macromol. Chem. Phys.* **2011**, *212*, 679.
(35) Bertin, D.; Gigmes, D.; Marque, S. R. A.; Tordo, P. *Chem. Soc. Rev.* **2011**, *40*, 2189.
(36) Fischer, H. *J. Polym. Sci., Part A: Polym. Chem.* **1999**, *37*, 1885.
(37) Tang, W.; Fukuda, T.; Matyjaszewski, K. *Macromolecules* **2006**, *39*, 4332.
(38) Nilsen, A.; Braslau, R. *J. Polym. Sci., Part A: Polym. Chem.* **2006**, *44*, 697.
(39) Mansfeld, U.; Hager, M. D.; Hoogenboom, R.; Ott, C.; Winter, A.; Schubert, U. S. *Chem. Commun.* **2009**, 3386.
(40) Dempwolf, W.; Flakus, S.; Schmidt-Naake, G. *Macromol. Symp.* **2009**, 275.
(41) Schulte, T.; Siegenthaler, K. O.; Luftmann, H.; Letzel, M.; Studer, A. *Macromolecules* **2005**, *38*, 6833.
(42) Karas, M.; Glückmann, M.; Schäfer, J. *J. Mass Spectrom.* **2000**, *35*, 1.
(43) Gründling, T.; Weidner, S.; Falkenhagen, J.; Barner-Kowollik, C. *Polym. Chem.* **2010**, *1*, 599.